scientific reports

Check for updates

OPEN

Synthesis and performance evaluation of polymer-ceramic composite microcapsules as reservoir protectant for natural gas hydrate drilling

Jintang Wang[1,2], Jiaqi Xu[1,2], Yujing Bai[1,2], Hao Xu[3]✉, Bo Liao[1,2], Guolei He[4], Yiyao Li[1,2] & Wenbiao Li[1,2]

Natural gas hydrate is a promising unconventional natural gas source due to its high energy density and huge global reserves. During exploitation, the drilling fluid may invade the hydrate formation and induce hydrate decomposition, causing reservoir damage. Herein, a novel reservoir protectant made by bio-degradable temporary plugging material (BDTPM) was developed in the form of polymer-ceramic composite microcapsules. As an additive to the drilling fluid, the BDTPM can minimize drilling fluid intrusion by plugging the reservoir during drilling and afterwards maximize permeability recovery by degrading the material. The particle size distribution was in the range of 1–130 μm. The optimal mass ratio between modified ceramic particles, ethyl cellulose and epoxy resin was found to be 4:2:1. The plugging rate was 100% when ethyl cellulose and epoxy resin were mixed to coat the ceramic particles to form BDTPM, and the plugging performance was the best. At a temperature close to the typical hydrate reservoir environment (5 °C), 0.02 wt% low-temperature complex enzyme can degrade BDTPM, and the permeability recovery rate is 64.66%. The efficient reservoir protectant developed in this work could play an important role in the successful drilling of natural gas hydrate reservoirs.

Keywords Natural gas hydrate, Drilling fluid, Temporary plugging material, Plugging removal, Permeability recovery

Natural gas hydrate has enormous reserves and worldwide distribution[1–5]. As a high-quality new energy source, natural gas hydrate has the advantages of high energy density, low exhaust pollution, environmental protection and non-toxic[6–10]. Rational development and utilization of natural gas hydrate will help ensure energy security, mitigate climate change and accelerate the sustainable development of energy. Submarine gas-hydrates are sensitive to temperature, pressure and foreign fluids. The exploitation of natural gas hydrates can be achieved by bringing the hydrate reservoir conditions outside the hydrate stability zone[11]. By expanding the mass and heat transfer area of the wellbore and reservoir in wells with complex structures such as horizontal wells, the hydrate decomposition rate can be effectively improved, natural gas recovery efficiency can be effectively improved, and hydrate production can be increased[12–14].

However, drilling fluid tends to infiltrate into the reservoir during the exploitation process, initiating hydrate decomposition[15]. This alteration of reservoir conditions subsequently triggers instability within the wellbore of the hydrate reservoir[16–18], ultimately resulting in damage to the reservoir. The exploitation of natural gas hydrate reservoirs is highly sensitive to thermal disturbances, as small temperature changes can lead to hydrate dissociation, potentially causing reservoir instability. Previous studies have thoroughly investigated the impact of temperature fluctuations on hydrate-bearing formations[19,20]. These works emphasize the necessity of maintaining thermal stability during drilling operations to avoid undesirable gas release and wellbore collapse. Similarly, Khurshid and Fujii[21] demonstrated how geomechanical changes caused by thermal disturbances further exacerbate the

[1]State Key Laboratory of Deep Oil and Gas, China University of Petroleum (East China), Qingdao 266580, China. [2]School of Petroleum Engineering, China University of Petroleum (East China), Qingdao 266580, China. [3]Qingdao Marine Equipment Inspection and Testing Group Co., Ltd., Offshore Engineering and Port Division, Qingdao 266000, China. [4]Institute of Exploration Techniques, Chinese Academy of Geosciences, Langfang 065000, Hebei, China. ✉email: xuhao@chinanmei.com

challenge of controlling gas hydrate dissociation during low-temperature drilling operations. The reservoir protectant prepared by the temporary plugging material can form a tight and stable "temporary plugging layer" to protect the reservoir and maintain the wellbore stable[22,23]. Microcapsules are widely used in various fields as a promising temporary plugging material[24–27]. Microcapsule is made of shell materials coated with core material to form a core-shell structure, which has isolation and protection performance and can improve compatibility and dispersion. Polymer-ceramic composite microcapsules are injected into the formation to form a plugging layer in the reservoir during the drilling process to stabilize the well wall and minimize natural gas hydrate decomposition. After the drilling is completed, the plugging layer can be degraded by biological enzymes and the permeability[28] can be restored for the benefit of hydrate exploitation.

Degradable temporary plugging materials have been widely used in oilfield production and operation due to their advantages, such as high plugging strength, good degradation effect, and environmental friendliness[29]. Xiong et al.[30] developed a degradable temporary plugging material with the advantages of high-temperature resistance, high strength, and good degradation effect. Zhang et al.[31] studied the effects of carrier fluid type, injection rate, crack width and crack morphology on the plugging behavior of degradable fibers and particles. Zhu et al.[32] developed a degradable preformed particle gel with excellent high-temperature resistance (150 ℃) and high salinity resistance (2,00,000 mg/L NaCl), which achieved plugging removal under reservoir conditions and was used in reservoir drilling and production. Zhong et al.[33] studied a temporary plugging material formed by combining degradable particles/powder gel with proppant. The temporary plugging material particles matched with formation particle size were pumped to plug the target fractures temporarily and degraded at high temperature for plugging removal, which can be applied to shale gas reservoirs. Zheng et al.[34] prepared an azo-type thermal crosslinking agent from azodisisobutyramidine hydrochloride (V-50) and maleic anhydride. On this basis, thermal-sensitive self-degradation microgels were prepared. The microgel particles are uniformly dispersed in the aqueous solution in the form of particles. The microgel was completely degraded within 5 h at 100 °C, and the residual amount of solid measured was 0. The temporary plugging materials discussed above are typically applied under relatively high temperatures (70–170 ℃), at present, there is a lack of research on degradable temporary plugging materials for low-temperature gas hydrate reservoirs. Therefore, it is imperative to develop an efficient reservoir protectant for natural gas hydrate drilling that can protect the reservoir during drilling and facilitate plug removal by biological enzymes after drilling[35,36].

In this work, a reservoir protectant for natural gas hydrate drilling made by bio-degradable temporary plugging material (BDTPM) in the form of polymer-ceramic composite microcapsules was developed. SEM, FTIR, particle size test and dispersion test characterized the coating effect of BDTPM. The effects of shell materials and core-shell ratio on the plugging performance of BDTPM were studied. The effects of biological enzymes on the plugging removal performance of BDTPM were tested. The advantages of BDTPM include low cost, easy access to the raw materials, simple and convenient preparation methods, and the prospect of large-scale industrial production. It can minimize drilling fluid intrusion by plugging the reservoir during drilling and maximize permeability recovery by degrading the material afterwards, which is of great significance for exploiting natural gas hydrate[37,38].

Experimental and methods

Materials

Epoxide resin E-51, ethyl cellulose, dichloromethane, Gelatin, Cellulase, and 3-aminopropyltrimethoxysilane were obtained from Shanghai Macklin Biochemical Co., Ltd. Ceramic particles were obtained from Sinopharm Chemical Reagent Co., Ltd. Amylase was obtained from Shanghai Aladdin Biochemical Technology Co., Ltd. Low-temperature complex enzyme was obtained from Cangzhou Zhonghe Zhongli Biological Products Co., Ltd.

Synthesis of BDTPM

Synthesis principle of BDTPM

In this experiment, synthesizing BDTPM included the coupling agent modification method[39–41] and the solvent evaporation method[42–45], with modified ceramic particles as the core and ethyl cellulose and epoxy resin as the shell materials. The driving forces were hydrogen bonds, covalent bonds, and physical crosslinking. The ceramic particles and silane coupling agent were connected by hydrogen bond, covalent bond and physical crosslinking, which coated the surface of the ceramic particles and modified them. The modified ceramic particles interacted with ethyl cellulose to form the hydrogen bond, thereby covering the surface of the modified ceramic particles. The epoxy resin and ethyl cellulose were polymerized to enhance the coating effect. Therefore, the feasibility of BDTPM prepared by coupling agent modification and solvent evaporation was theoretically supported.

The Si–OH formed during the hydrolysis of the silane coupling agent forms the hydrogen bond with the –OH on the surface of the ceramic particles[46]. A dehydration condensation reaction generated the Si-O-Si covalent bond. The silane coupling agent was coated on the surface of the ceramic particles to obtain modified ceramic particles with hydrophobic properties. The Si–OH in the modified ceramic particles forms the hydrogen bond with the –OH in the ethyl cellulose, forming the covalent bond as an intermediate bridge between the modified ceramic particles and the shell materials, connecting the modified ceramic particles with ethyl cellulose. Based on ethyl cellulose's hydrogen bond and covalent bond, and the polymerization of ethyl cellulose with epoxy resin[47], BDTPM with high-efficiency plugging and plugging removal performance can be formed.

Synthesis method of BDTPM

The preparation process of BDTPM is shown in Fig. 1.

Preparation of modified ceramic particles. The silane coupling agent solution was obtained by mixing 1 mL of 3-aminopropyltrimethoxysilane with 100 mL of deionized water at room temperature[48]. The mass ratio of ceramic particles and silane coupling agent was maintained at 20:1. The 20 g ceramic particles were fully

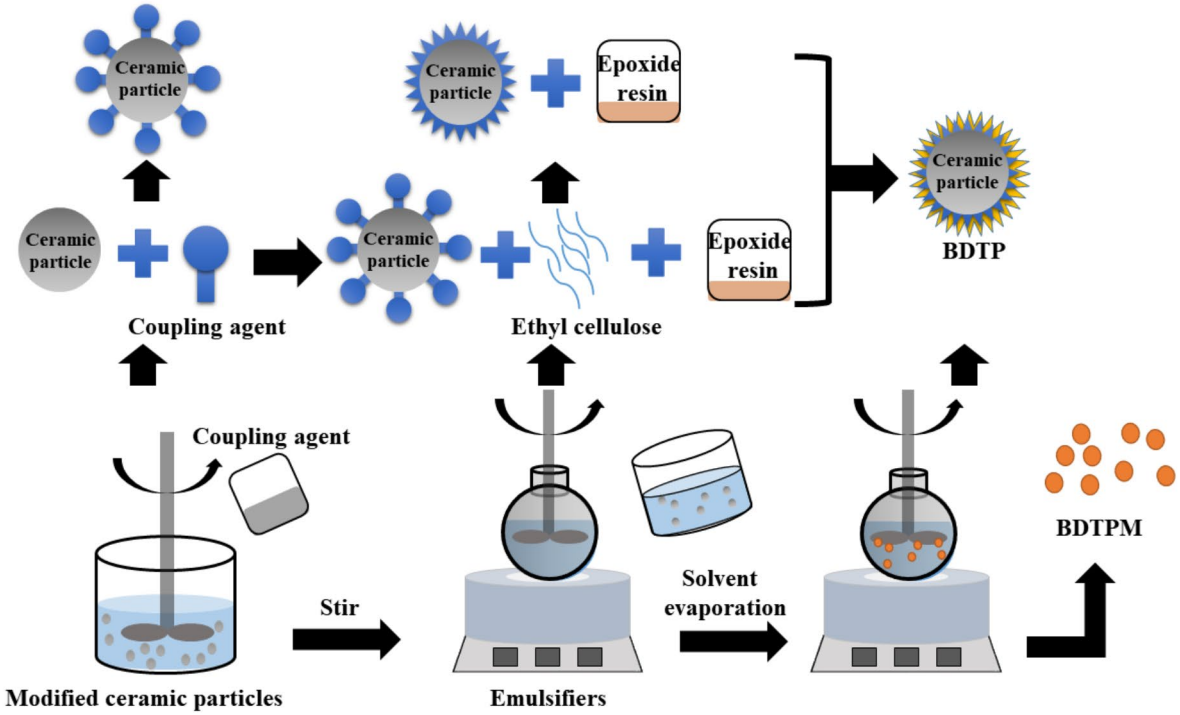

Fig. 1. The synthesis procedure of BDTPM.

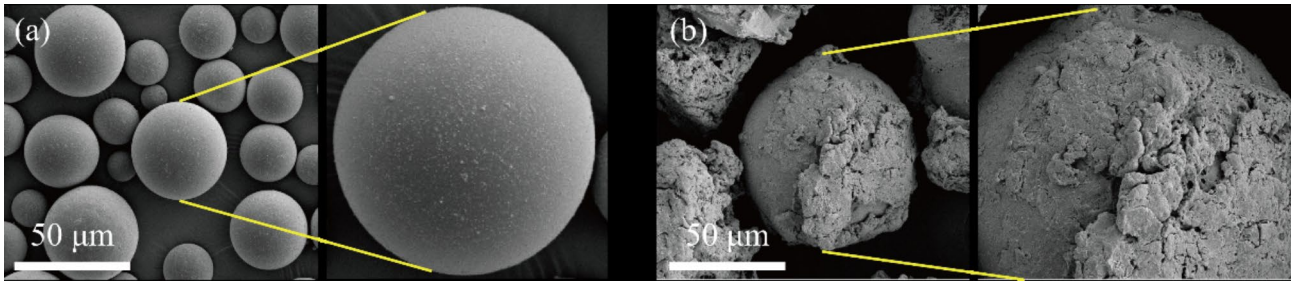

Fig. 2. SEM images of (**a**) ceramic particles and (**b**) BDTPM.

dispersed in silane coupling agent solution and stirred for 40 min at a stirring rate of 200 rpm. The modified ceramic particles were obtained by drying.

Preparation of BDTPM. 1 g of gelatin was dissolved in 100 mL of deionized water, and a gelatin aqueous solution was formed by heating and stirring as the aqueous phase. The stirring temperature was 30 °C, and the stirring rate was 200 rpm. 20 g of modified ceramic particles, 5 g ethyl cellulose, and 2.5 g epoxy resin were dissolved in 100 g dichloromethane at a mass ratio of 4:2:1, and the mass ratio of modified ceramic particles and dichloromethane was 1:50. The mixed solution was formed as the oil phase by stirring. The stirring rate was 200 rpm, and the stirring temperature was room temperature. The oil phase was added to the water phase, mixed evenly, and stirred continuously for 5 h at room temperature, and the stirring rate was 200 rpm. The temperature was raised to 50 °C, stirred for 2 h, washed 3 times with deionized water, and dried at 70 °C to 80 °C for 12 h to obtain BDTPM.

Results and discussion

Characterization of BDTPM

SEM characterization

The surface morphology of the BDTPM samples prepared by the coupling agent modification method and the solvent evaporation method is observed by SEM, as shown in Fig. 2. It can be seen from Fig. 2b that the surface of the particles gradually becomes rough and covered with a coating layer after the ceramic particles are coated by the coupling agent surface modification and solvent evaporation, which would plug the pores of the ceramic particles and make the BDTPM have plugging performance. The roughness of the particle surface is due to the irregular coating formed by covalent bonds and polysaccharides.

Infrared spectroscopic characterization

An infrared spectrometer is used to characterize BDTPM in the range of 500 to 4000 cm^{-1}, as shown in Fig. 3. In the FTIR of ceramic particles[49], the stretching vibration peak of –OH exists at 3441.05 cm^{-1}, and the stretching vibration peaks of –CH exist at 2928.92 cm^{-1} and 2853.81 cm^{-1}. Meanwhile, the stretching vibration peak of –C=C exists at 1639.35 cm^{-1}. In the FTIR of coupling agent[50], the stretching vibration peak of –OH is at 3572.27 cm^{-1}, and the stretching vibration peak of –CH of propyl is at 1381.78 cm^{-1}. In the FTIR of ethyl cellulose[51], we can see that the peaks at 3473.24 cm^{-1} and 1642.27 cm^{-1} are the stretching vibration peaks of –OH, –C=C, while the peaks at 2971.85 cm^{-1} and 2865.52 cm^{-1} are –CH stretching vibration peaks of methyl and methylene. Moreover, the characteristic peaks of ethyl and fatty ether are at 1368.17 cm^{-1} and 1115.52 cm^{-1}. In the FTIR of epoxy resin[52], there is a stretching vibration peak of –OH at 3618.58 cm^{-1} and a stretching vibration peak of –C=C at 1683.24 cm^{-1}. In the FTIR of BDTPM, we can see that the peaks at 3495.68 cm^{-1} and 1656.91 cm^{-1} are the stretching vibration peaks of –OH and –C=C, while the stretching vibration peaks of –CH at 2979.65 cm^{-1} and 2873.32 cm^{-1}. At the same time, the characteristic peaks of propyl, ethyl, and fatty ether are at 1380.98 cm^{-1}, 1360.23 cm^{-1}, and 1115.52 cm^{-1}.

It is evident that the stretching vibration peaks of –OH, –CH, and –C=C in BDTPM and ceramic particles. Stretching vibration peaks of --OH and propyl characteristic peaks are present in both BDTPM and coupling agents. Additionally, the stretching vibration peaks of –OH, –CH, –C=C, ethyl, and fatty ether are present in BDTPM and ethyl cellulose. Finally, the stretching vibration peaks of –OH and –C=C exist in BDTPM and epoxy resin. It has been proven that BDTPM, which contains ceramic particles, coupling agents, ethyl cellulose, and epoxy resin, has been successfully synthesized.

Particle size test characterization

A laser particle size analyzer measures the particle size distribution of BDTPM. The cumulative particle size distribution curve and histogram of ceramic particles and BDTPM at D_{10}, D_{50}, and D_{90} are shown in Fig. 4. The median particle size of the ceramic particles is 44 μm, while the median particle size of BDTPM is 70 μm. It indicates that the particle size of polymer-ceramic composite microcapsules prepared by coating ceramic particles from shell materials increases, the particle size of BDTPM is larger than the ceramic particles, and the overall distribution of BDTPM is in the range of 1 to 130 μm. Moreover, D_{10} increases from 23.6 μm to 26.6 μm and D_{90} increases from 99 μm to 132 μm. Thus, the particle size of BDTPM increases obviously with the surface

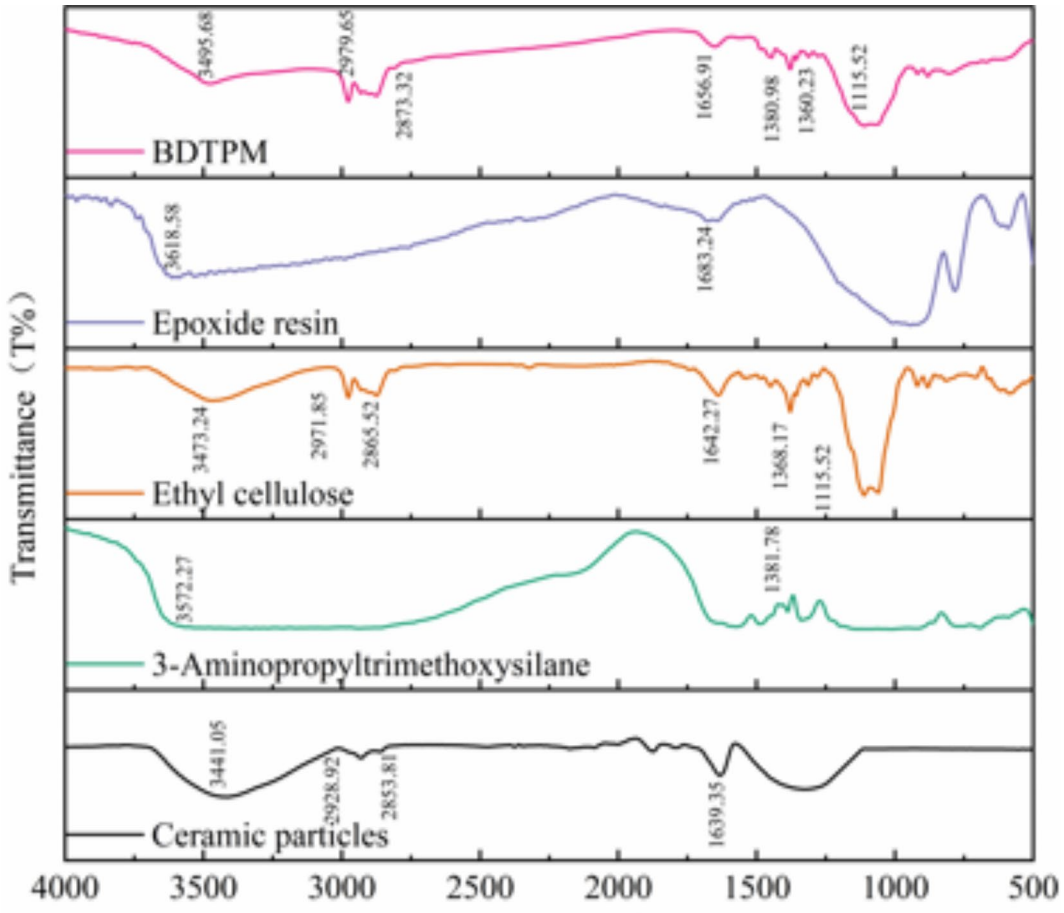

Fig. 3. FTIR of ceramic particles, 3-aminopropyltrimethoxysilane, ethyl cellulose, epoxy resin, BDTPM.

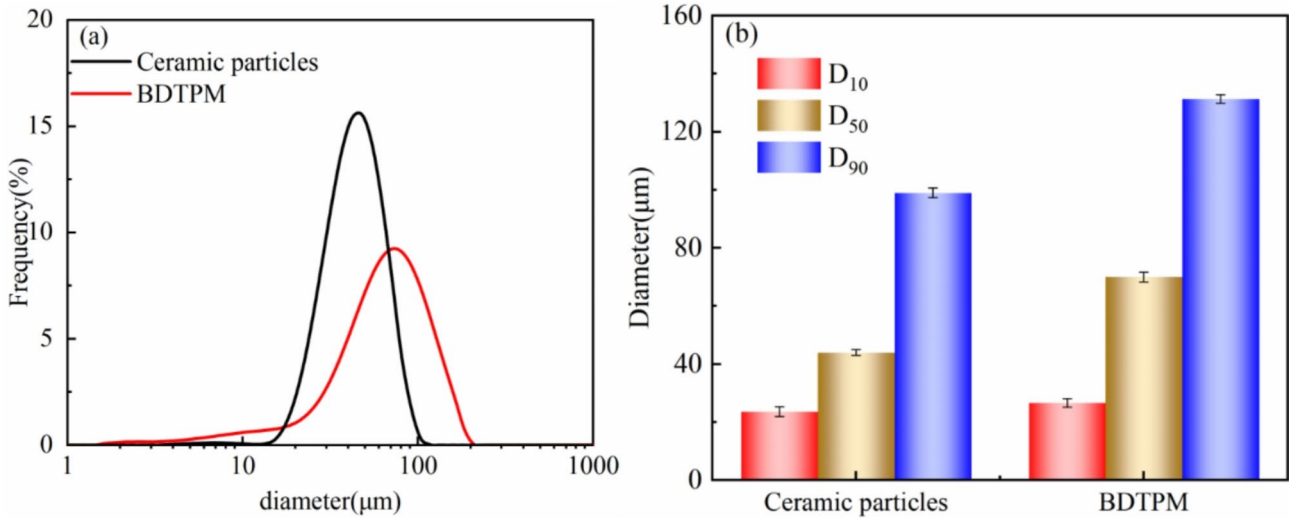

Fig. 4. The size distributions of ceramic particles and BDTPM: (**a**) Cumulative particle size distribution curve, (**b**) Histogram of ceramic particles and BDTPM at D_{10}, D_{50}, D_{90}.

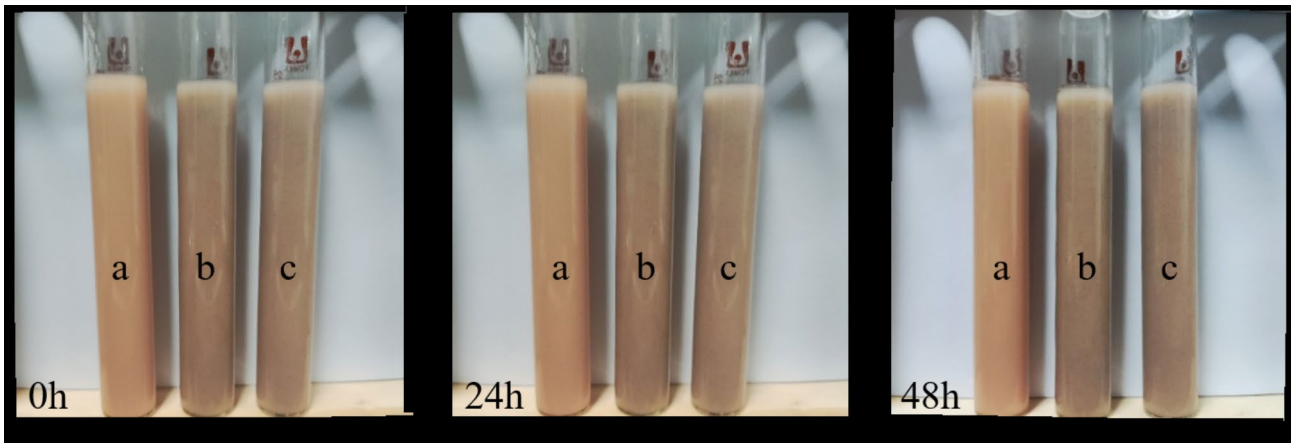

Fig. 5. Stability of ceramic particles (3%) and BDTPM (4%) in 4% water-based bentonite at different times: (**a**) 4% bentonite, (**b**) 3% ceramic particles + 4% bentonite, (**c**) 3% BDTPM + 4% bentonite.

Material	Density (g/cm³)	
	Supernatant	Subnatant
4% bentonite	1.021	1.021
3% ceramic particles + 4% bentonite	1.058	1.058
3% BDTPM + 4% bentonite	1.062	1.062

Table 1. The density of water-based drilling fluid.

of the ceramic particles covered by the shell materials, which indicates that the shell materials cover the ceramic particles effectively.

Dispersion performance test

The dispersion of ceramic particles (3%) and BDTPM (3%) in 4% water-based bentonite is tested within 48 h, as shown in Fig. 5. Obviously, the color of both solutions changed and darker, but the dispersion of those kept stability at 48 h. It means the ceramic particles and BDTPM could be stably dispersed in the 4% water-based bentonite after 48 h of static observation. Moreover, the density of supernatant and the subnatant in the drilling fluid are also tested, as shown in Table 1. The densities of the supernatant and subnatant in bentonite, ceramic particles/bentonite system, and bentonite/BDTPM system are 1.021 g/cm³, 1.058 g/cm³, and 1.062 g/cm³,

respectively. It indicated that the density of the supernatant and the subnatant in all systems have little difference, and the dispersion effect of ceramic particles and BDTPM is good.

BDTPM plugging performance

The effects of the shell materials on BDTPM

To investigate the effects of the shell materials on modified ceramic particles, BDTPM was prepared with different shell materials, including modified ceramic particles, ethyl cellulose, epoxy resin, and ethyl cellulose/epoxy resin. First, the initial permeability[53–55] of the core is tested, and then 6 g of BDTPM is plugged into the front of the core. The permeability of the core plugged by BDTPM is tested, and the plugging effect of different materials is compared, as shown in Fig. 6. When modified ceramic particles are used, the initial core permeability and permeability of the core plugged by microcapsules are 1.527×10^{-3} μm^2 and 0.942×10^{-3} μm^2. Meanwhile, the plugging rate of 38.31% indicates that the plugging effect of the modified ceramic particles is poor. When single ethyl cellulose is used as a shell material to wrap modified ceramic particles, the initial core permeability and permeability of the core plugged by BDTPM are 0.726×10^{-3} μm^2, 0.459×10^{-3} μm^2. Thus, the plugging rate is 36.78%, which shows that BDTPM wrapped by single shell material has a poor plugging effect. When the single epoxy resin is used as a shell material to cover the modified ceramic particles, the initial core permeability and permeability of the core plugged by BDTPM are 1.313×10^{-3} μm^2, 0.621×10^{-3} μm^2, the plugging rate of 52.70%. BDTPM is formed when ethyl cellulose and epoxy resin are mixed and wrapped in modified ceramic particles. The initial core permeability and permeability of the core plugged by BDTPM are 1.74×10^{-3} μm^2, 0×10^{-3} μm^2, as well as the plugging rate rises to 100%, which can completely plug the core and have an excellent plugging effect.

Ethyl cellulose and epoxy resin are mixed to cover modified ceramic particles to prepare BDTPM. The Silane coupling agent connects ceramic particles and ethyl cellulose by forming covalent bonds, so the material possesses a specific plugging effect. The solvent evaporation method can polymerize the ethyl cellulose and epoxy resin to form a better coating layer, preventing foreign fluid from invading the reservoir and enhancing the plugging effect.

The effects of shell ratio of core on modified ceramic particles

The sandbed instrument tests the plugging performance of BDTPM (modified ceramic particles, ethyl cellulose, epoxy resin with a mass ratio of 2:2:1, 4:2:1, 8:2:1). At the same time, the plugging effect of BDTPM is evaluated. The drilling fluid intrusion depth of bentonite and BDTPM / bentonite system is tested. Through experimental analysis, the depth of bentonite (4%) intrusion into 60-mesh to 80-mesh quartz sand is 18 cm, as shown in Table 2. Therefore, bentonite (4%) seepage from quartz sand indicates no plugging ability. After adding BDTPM (2:2:1) to bentonite (4%), the intrusion depth is 5 cm. The drilling fluid has a plugging performance, which can plug quartz sand. After adding BDTPM (4:2:1) to bentonite (4%), the intrusion depth is 3.5 cm, so the intrusion rate is reduced from 27.78 to 19.44%, which significantly reduces the intrusion depth, enhances the plugging performance of drilling fluid, and shows significant plugging effect. The plugging performance of drilling fluid is enhanced, and the plugging effect is remarkable. The intrusion depth and rate are 4 cm and 22.22% when BDTPM (8:2:1) is added to bentonite (4%). Compared with the BDTPM (4:2:1), the intrusion depth of BDTPM (8:2:1) increases. However, the intrusion rate of BDTPM (8:2:1) increases slightly, which results in a decline in the plugging performance of drilling fluid. In contrast, bentonite (4%) has no plugging effect. With the addition of BDTPM of different proportions, drilling fluid has an excellent plugging effect to prevent drilling

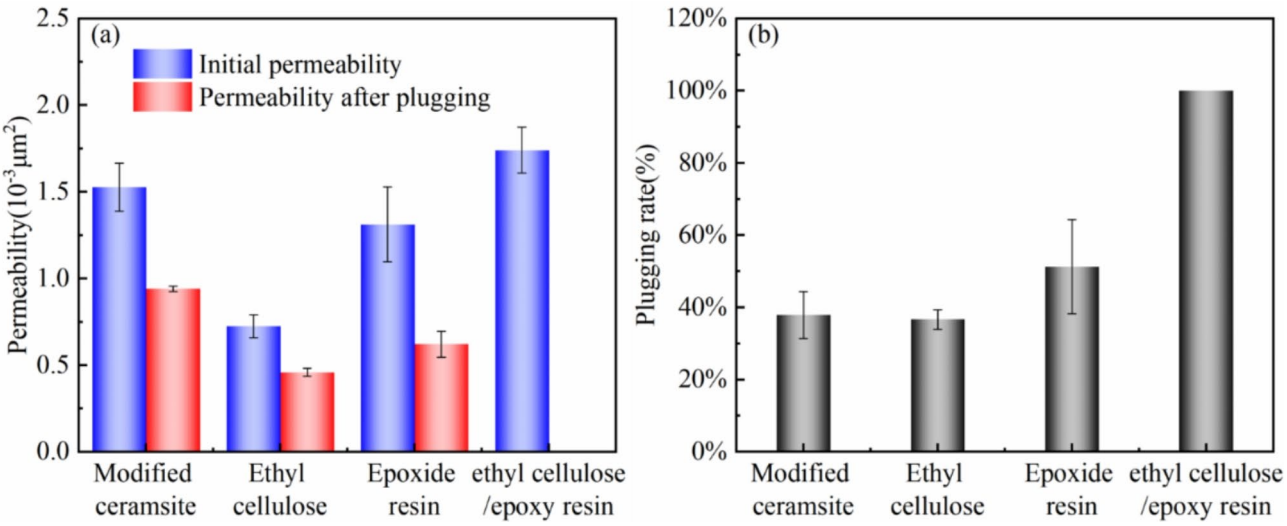

Fig. 6. Permeability and plugging rate before and after core plugged by microcapsules: (**a**) Permeability change chart of microcapsules under different shell materials, (**b**) Plugging rate of microcapsules under different shell materials.

Material	Core-shell ratio	Intrusion depth(cm)	Intrusion rate(%)
4% bentonite	–	18	100
4% bentonite	2:2:1	5	27.78
4% bentonite	4:2:1	3.5	19.44
4% bentonite	8:2:1	4	22.22

Table 2. Performance of sandbed plugging.

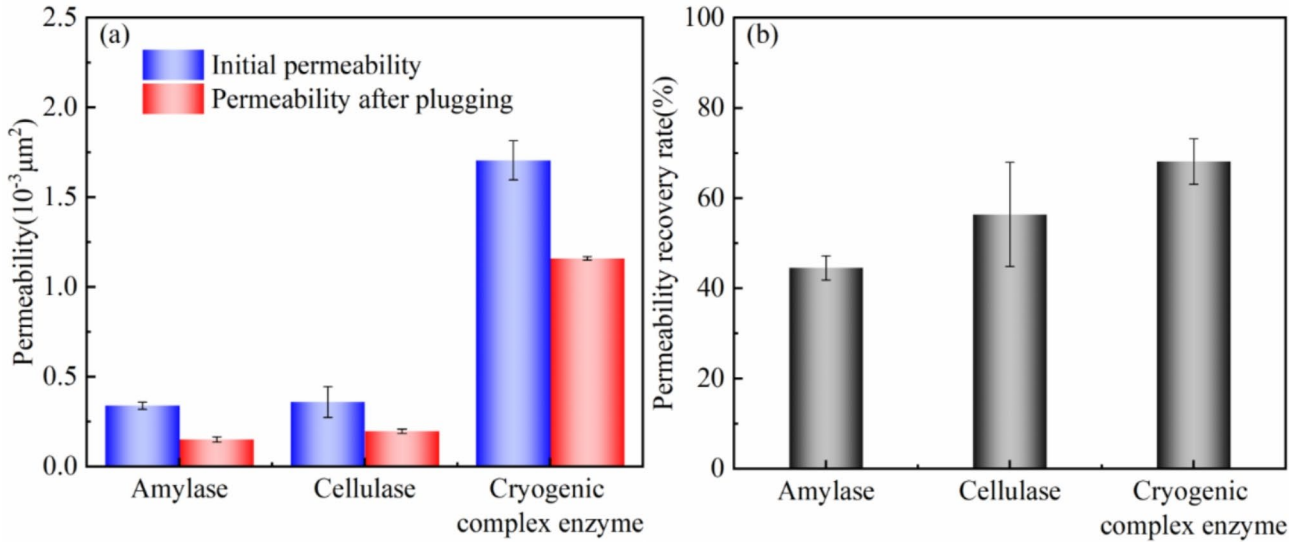

Fig. 7. Permeability and permeability recovery rate of the core after 24 h degradation of BDTPM by the enzyme at 5 °C: (**a**) Permeability change plot, (**b**) Permeability recovery rate plot.

fluid from invading quartz sand. After adding BDTPM (4:2:1), the intrusion depth is minimal, and the plugging performance is strongest.

The plugging removal performance of BDTPM

The effects of biological enzyme on BDTPM

The ambient temperature of the gas hydrate reservoirs in the sea area is between 0 and 20 ℃[56,57]. Usually, the lower the temperature, the worse the enzyme activity. First, the initial permeability of the core is tested. Second, BDTPM was degraded by 0.2 wt% amylases, 0.2 wt% cellulases and 0.2 wt% low-temperature complex enzymes at 5 °C for 24 h. Then, the BDTPM degraded by 6 g enzymes is plugged into the front of the core. Finally, the permeability recovery rate of the core plugged by BDTPM is tested, as shown in Fig. 7. The temporary plugging effect of BDTPM in the core is tested after 24 h degradation by amylase. The results show that the initial permeability of the core and permeability of the core plugged by BDTPM are 0.34×10^{-3} μm^2 and 0.152×10^{-3} μm^2, and the permeability recovery rate is 44.70%. Thus, amylase has poor degradation performance on BDTPM at low temperatures. The temporary plugging effect of BDTPM in the core is tested after 24 h degradation by cellulase. The consequences indicate that the initial permeability and permeability of the core plugged by BDTPM are 0.36×10^{-3} μm^2 and 0.197×10^{-3} μm^2, and the permeability recovery rate is 54.72%. Thus, the degradation ability of cellulase on BDTPM increases at low temperatures. Meanwhile, the temporary plugging effect of BDTPM in the core is tested after 24 h degradation by the low-temperature complex enzyme. The results show that the initial permeability and permeability of the core plugged by BDTPM are 1.707×10^{-3} μm^2 and 1.160×10^{-3} μm^2, and the permeability recovery rate is 67.95%. Hence, the low-temperature complex enzyme has the best degradation ability for BDTPM at low temperatures. Compared with amylase and cellulase, the low-temperature complex enzyme has better enzymatic activity at 5 °C, which can degrade the shell of BDTPM, thereby opening the pore channel and realizing the plugging removal of BDTPM under the action of the biological enzyme.

At 10 ℃, 0.2 wt% amylases, 0.2 wt% cellulases and 0.2 wt% low-temperature complex enzymes are used to degrade BDTPM for 24 h, respectively. The permeability recovery rate of the core plugged by BDTPM is tested, as shown in Fig. 8. The temporary plugging effect of BDTPM is tested after being degraded by amylase for 24 h. The results show that the initial permeability and permeability of the core plugged by BDTPM are 0.43×10^{-3} μm^2 and 0.195×10^{-3} μm^2, and the permeability recovery rate is 45.35%. Therefore, the degradation effect of amylase is weak, and channels of BDTPM cannot be fully opened. After 24 h of degradation of BDTPM by cellulase, the temporary plugging effect of the core is tested. The consequences indicate that the initial permeability and permeability of the core plugged by BDTPM are 0.382×10^{-3} μm^2 and 0.196×10^{-3} μm^2, and the recovery rate of permeability is 51.30%. So, the degradation ability of cellulase on BDTPM is enhanced, indicating that the effect

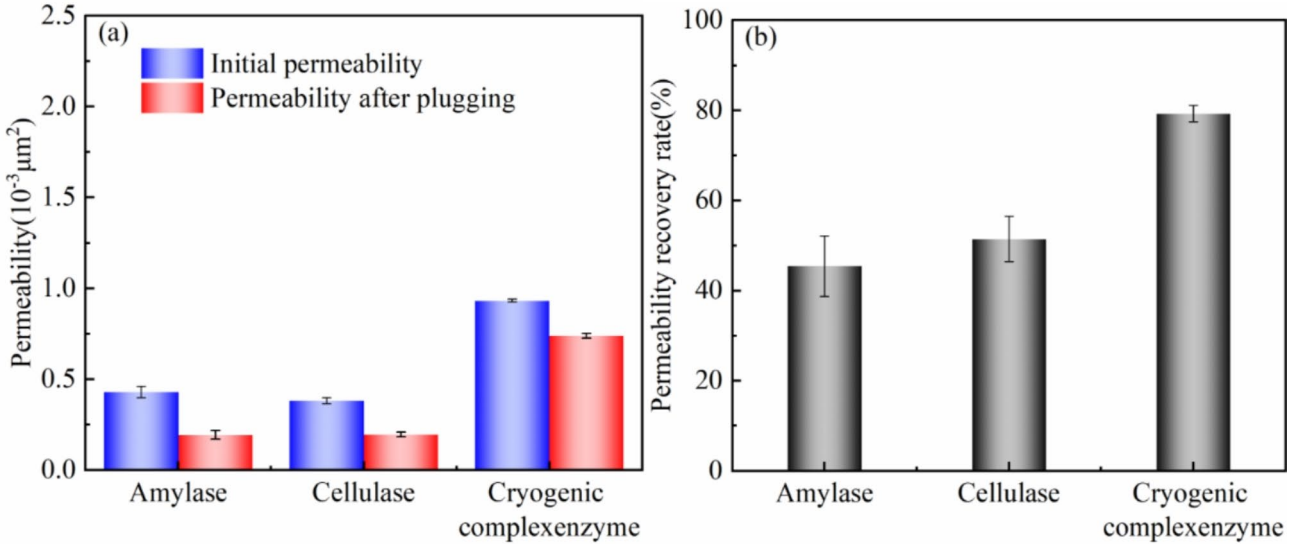

Fig. 8. Permeability and permeability recovery rate of the core after 24 h degradation of BDTPM by the enzyme at 10 °C: (**a**) Permeability change plot, (**b**) Permeability recovery rate plot.

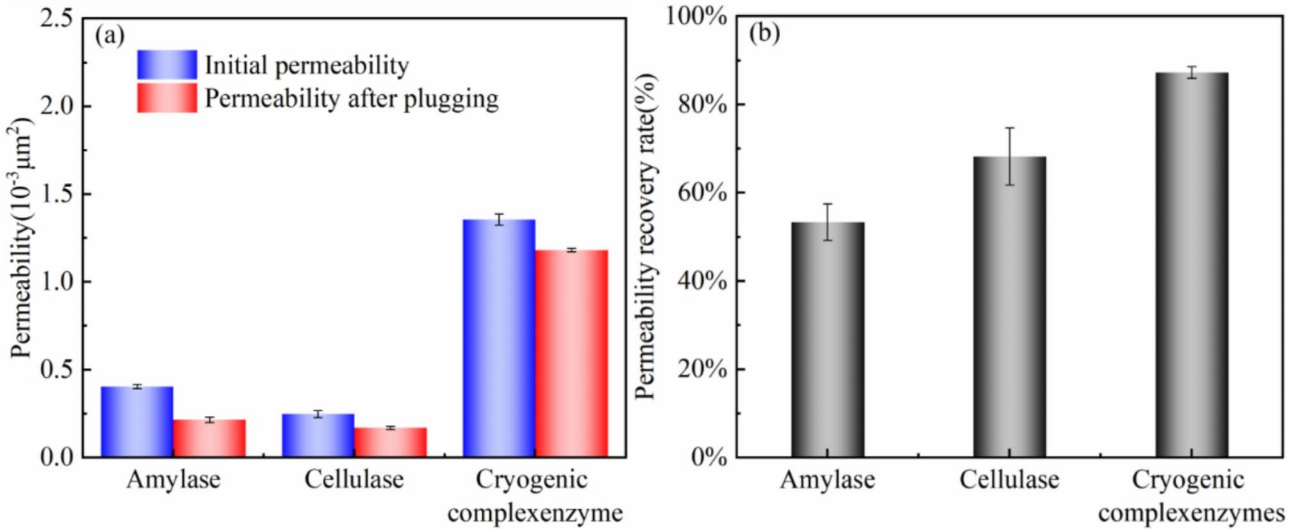

Fig. 9. Permeability and permeability recovery rate of the core after 24 h degradation of BDTPM by the enzyme at 15 °C: (**a**) Permeability change plot, (**b**) Permeability recovery rate plot.

of the enzyme is significant with an increase in temperature. After 24 h of low-temperature complex enzyme degradation, the temporary plugging effect of the core is tested. The results indicate that the initial permeability and permeability of the core plugged by BDTPM are 0.933×10^{-3} μm^2 and 0.739×10^{-3} μm^2, and the permeability recovery rate is 79.21%. At 10 ℃, the degradation effect of the low-temperature complex enzyme is the best, and the permeability recovery rate after plugging is the highest. BDTPM is effectively suitable for the plugging removal of BDTPM.

At 15 ℃, 0.2 wt% amylases, 0.2 wt% cellulases, and 0.2 wt% low-temperature complex enzymes are used to degrade BDTPM for 24 h, respectively, and the permeability recovery rate of the core plugged by BDTPM is tested, as shown in Fig. 9. The temporary plugging effect of the material is tested after 24 h of degradation of BDTPM by amylase. The results show that the initial permeability and permeability of the core plugged by BDTPM are 0.405×10^{-3} μm^2 and 0.216×10^{-3} μm^2, and the permeability recovery rate is 53.33%. Thus, the degradation effect of amylase is poor. The temporary plugging effect of the core is tested after 24 h of degradation of BDTPM by cellulase. The consequences indicate that the initial permeability and permeability of the core plugged by BDTPM are 0.248×10^{-3} μm^2 and 0.169×10^{-3} μm^2, and the permeability recovery rate is 68.15%. The temporary plugging effect of the core is tested after 24 h of degradation of BDTPM by the low-temperature complex enzyme. The results show that the initial permeability and permeability of the core plugged by BDTPM

are 1.355×10^{-3} μm^2 and 1.182×10^{-3} μm^2, and the permeability recovery rate is 87.23%. As the activity of biological enzymes is affected by temperature, the degradation performance of biological enzymes is enhanced with the increase in temperature. The permeability recovery rate of the core plugged by BDTPM gradually increases under the action of amylase, cellulase, and low-temperature complex enzyme when the degradation temperature of the biological enzyme is 5 ℃, 10 ℃, 15 ℃. Hence, the permeability recovery rate under the action of low-temperature complex enzymes is the highest at different temperatures. Meanwhile, the permeability recovery rate changes significantly. The low-temperature complex enzyme matching with the temperature of hydrate reservoirs[58] is applicable to hydrate reservoir plugging removal. Therefore, the low-temperature complex enzyme is selected for the plugging removal of BDTPM.

The effects of low-temperature complex enzyme concentration on BDTPM

The low-temperature complex enzymes of 0.02 wt%, 0.2 wt%, and 2 wt% are selected to degrade BDTPM at 5 °C for 24 h, and the permeability recovery rate of the core plugged by BDTPM is tested, as shown in Fig. 10. The permeability recovery rate is 64.66% when the low-temperature complex enzyme concentration is 0.02 wt%. Next, the permeability recovery rate is 67.94% when the low-temperature complex enzyme concentration is 0.2 wt%. In the meantime, the permeability recovery rate is 90.92 wt% when the concentration is 2 wt%. As the concentration of low-temperature complex enzyme changes from 0.02 wt% to 0.2 wt%, the range of variation of permeability of the core plugged by BDTPM is low. However, BDTPM degraded by low-temperature complex enzyme has a high permeability recovery rate. The low-temperature complex enzyme can realize the plugging removal of BDTPM. When the concentration is 2 wt%, the permeability recovery rate is the highest and the degradation effect is the best. However, the dosage of biological enzymes is too much. At a temperature close to the typical hydrate reservoir environment (5 °C), a low dosage (0.02 wt%) of low-temperature complex enzyme was found to be good enough to degrade the plugging material and recover permeability. Therefore, 0.02 wt% low-temperature complex enzyme with less amount and low cost is used to remove BDTPM at 5 °C, which is suitable for temporarily plugging hydrate reservoirs.

Conclusion

In this work, a novel reservoir protectant for natural gas hydrate drilling (BDTPM) was developed. BDTPM was prepared by the coupling agent modification method and the solvent evaporation method with modified ceramic particles as the core and ethyl cellulose and epoxy resin as the shell materials. It can be plugged into the reservoir during the drilling process and degraded by biological enzymes after drilling. The median particle size of the ceramic particles is 44 μm, while the median particle size of BDTPM is 70 μm. The particle size of BDTPM is larger than the ceramic particles, and its overall distribution is in the range of 1 to 130 μm. The shell material is coated with ceramic particles. The plugging rate was 100% when ethyl cellulose and epoxy resin were mixed to coat the ceramic particles to form BDTPM, and the plugging performance was the best. The optimal mass ratio between modified ceramic particles, ethyl cellulose, and epoxy resin was found to be 4:2:1, and the drilling fluid intrusion (3% BDTPM/4% bentonite) was 3.5 cm. At a temperature close to the typical hydrate reservoir environment (5 °C), 0.02 wt% low-temperature complex enzyme can degrade BDTPM, and the permeability recovery rate is 64.66%.

Data availability

The data supporting this study's findings are available from the corresponding author upon reasonable request.

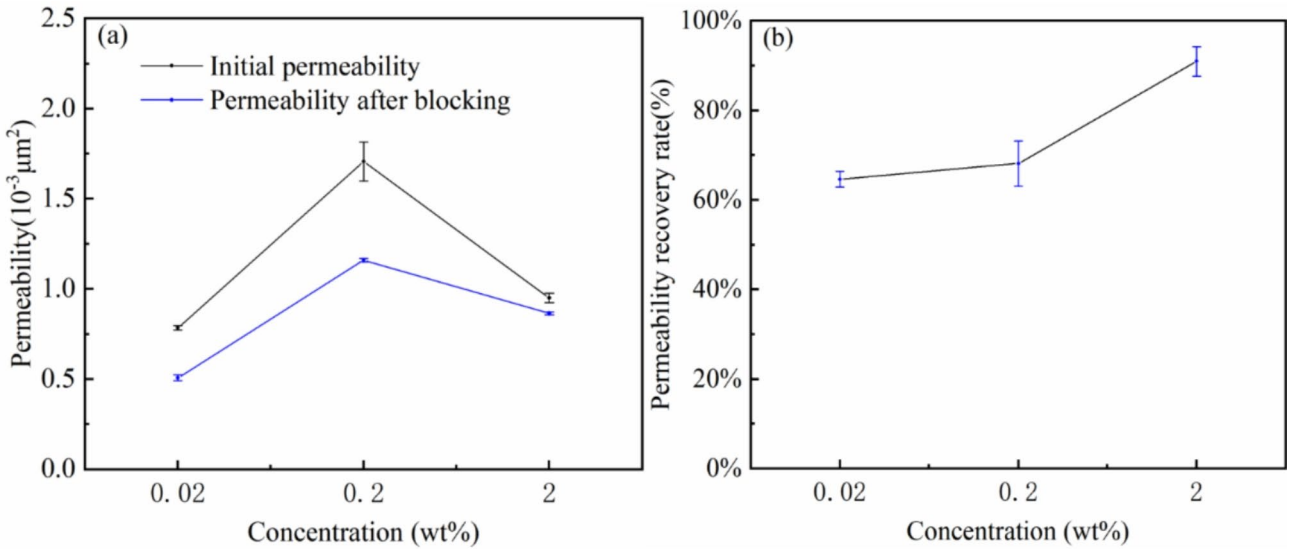

Fig. 10. Permeability and permeability recovery rate of the core after 24 h degradation of BDTPM by bio-enzyme at 5 °C: (**a**) Permeability change plot, (**b**) Permeability recovery rate plot.

Received: 3 June 2024; Accepted: 17 September 2024
Published online: 30 September 2024

References

1. Liao, B. et al. Microscopic insights into synergism effect of different hydrate inhibitors on methane hydrate formation: Experiments and molecular dynamics simulations. *Fuel*. https://doi.org/10.1016/j.fuel.2023.127488 (2023).
2. Liu, J.-W. & Li, X.-S. Recent advances on natural gas hydrate exploration and development in the South China Sea. *Energy Fuels* **35**, 7528–7552 (2021).
3. Jianliang, Y. et al. Main progress of the second gas hydrate trial production in the South China Sea. *Geol. China* **47**, 557–568 (2020).
4. Liao, B. et al. Microscopic molecular insights into clathrate methane hydrates dissociation in a flowing system. *Chem. Eng. J.* **430**, 133098 (2022).
5. Li, G., Moridis, G. J., Zhang, K. & Li, X.-S. Evaluation of gas production potential from marine gas hydrate deposits in Shenhu area of South China Sea. *Energy Fuels* **24**, 6018–6033 (2010).
6. Li, F. et al. A review: Enhanced recovery of natural gas hydrate reservoirs. *Chin. J. Chem. Eng.* **27**, 2062–2073 (2019).
7. Song, Y. et al. The status of natural gas hydrate research in China: A review. *Renew. Sustain. Energy Rev.* **31**, 778–791 (2014).
8. Lee, S.-Y. & Holder, G. D. Methane hydrates potential as a future energy source. *Fuel Process. Technol.* **71**, 181–186 (2001).
9. Li, Z. et al. Kinetic mechanisms of methane hydrate replacement and carbon dioxide hydrate reorganization. *Chem. Eng. J.* **477**, 146973 (2023).
10. Khurana, M., Yin, Z. & Linga, P. A review of clathrate hydrate nucleation. *ACS Sustain. Chem. Eng.* **5**, 11176–11203 (2017).
11. Wang, Y. et al. Reservoir formation damage during hydrate dissociation in sand-clay sediment from Qilian Mountain permafrost, China. *Appl. Energy* **263**, 114619 (2020).
12. Sun, W., Li, G., Qin, H., Li, S. & Xu, J. Enhanced gas production from class II gas hydrate reservoirs by the multistage fractured horizontal well. *Energies* **16**, 3354 (2023).
13. Huang, M. et al. Improving the production performance of low-permeability natural gas hydrate reservoirs by radial water jet slotting and grouting in a horizontal well. *Energy Fuels* **37**, 7715–7727 (2023).
14. Wang, J. et al. Development of a dual-functional inhibitor for natural gas hydrates and construction of drilling fluid system. *Gas Sci. Eng.* **122**, 205218 (2024).
15. Wang, Q. et al. Effect of drilling fluid invasion on natural gas hydrate near-well reservoirs drilling in a horizontal well. *Energies* **14**, 7075 (2021).
16. Zhi, Z. et al. Influence of deep-water well production system on natural gas hydrate decomposition. *Acta Petrol. Sin.* **43**, 281.
17. Tianle, L. et al. Negative effect of cementing slurry invasion on gas hydrate stability around borehole wall. *Acta Petrol. Sin.* **39**, 937 (2018).
18. Wang, J. et al. The effect of multi-component inhibitor systems on hydrate formation. *Gas Sci. Eng.* **122**, 205214 (2024).
19. Khurshid, I., Lee, K. J. & Choe, J. Analyses of thermal disturbance in drilling deep and high temperature formations. *Energy Sources Part A Recovery Util. Environ. Effects* **35**, 1487–1497. https://doi.org/10.1080/15567036.2010.529562 (2013).
20. Sun, J. et al. Wellbore stability analysis during drilling through marine gas hydrate-bearing sediments in Shenhu area: A case study. *J. Petrol. Sci. Eng.* **170**, 345–367. https://doi.org/10.1016/j.petrol.2018.06.032 (2018).
21. Khurshid, I. & Fujii, Y. Geomechanical analysis of formation deformation and permeability enhancement due to low-temperature CO2 injection in subsurface oil reservoirs. *J. Petrol. Explor. Prod. Technol.* **11**, 1915–1923. https://doi.org/10.1007/s13202-021-01133-1 (2021).
22. Chen, Z. et al. Optimization of degradable temporary plugging material and experimental study on stability of temporary plugging layer. *Front. Phys.* **11**, 1167215 (2023).
23. Sun, J. et al. Development and performance evaluation of bioenzyme-responsive temporary plugging materials. *Adv. Geo-Energy Res.* **11**, 20–28 (2024).
24. Bah, M. G., Bilal, H. M. & Wang, J. Fabrication and application of complex microcapsules: A review. *Soft Matter* **16**, 570–590 (2020).
25. Remunan-Lopez, C., Lorenzo-Lamosa, M., Vila-Jato, J. & Alonso, M. Development of new chitosan–cellulose multicore microparticles for controlled drug delivery. *Eur. J. Pharm. Biopharm.* **45**, 49–56 (1998).
26. Andersson, C. et al. Preparation and incorporation of microcapsules in functional coatings for self-healing of packaging board. *Packag. Technol. Sci.* **22**, 275–291 (2009).
27. Shum, H. C., Kim, J.-W. & Weitz, D. A. Microfluidic fabrication of monodisperse biocompatible and biodegradable polymersomes with controlled permeability. *J. Am. Chem. Soc.* **130**, 9543–9549 (2008).
28. Lall, D., Vishal, V., Tulsawadekar, K., Dixit, G. & PG, R. Effect of permeability reduction on the production of a gas hydrate reservoir during horizontal depressurization. *Energy Fuels* (2024).
29. Wang, D. et al. An experimental study on the mechanism of degradable fiber-assisted diverting fracturing and its influencing factors. *J. Nat. Gas Sci. Eng.* **27**, 260–273. https://doi.org/10.1016/j.jngse.2015.08.062 (2015).
30. Xiong, C. et al. High efficiency reservoir stimulation based on temporary plugging and diverting for deep reservoirs. *Petrol. Explor. Dev.* **45**, 948–954 (2018).
31. Zhang, L. et al. Experimental study on plugging behavior of degradable fibers and particulates within acid-etched fracture. *J. Petrol. Sci. Eng.* **185**, 106455 (2020).
32. Zhu, D.-Y. et al. Development of degradable pre-formed particle gel (DPPG) as temporary plugging agent for petroleum drilling and production. *Petrol. Sci.* **18**, 479–494 (2021).
33. Zhong, Y. et al. A composite temporary plugging technology for hydraulic fracture diverting treatment in gas shales: Using degradable particle/powder gels (DPGs) and proppants as temporary plugging agents. *J. Petrol. Sci. Eng.* **216**, 110851 (2022).
34. Zheng, C. et al. Preparation, properties, and degradation mechanism of thermosensitive self-degradation microgel. *J. Dispers. Sci. Technol.* **44**, 1216–1225 (2023).
35. Sun, J. et al. Research progress and application prospects of smart materials in lost circulation control of drilling fluids. *J. China Univ. Pet.* **4**, 100–110 (2020).
36. Wang, R. et al. Preparation and investigation of self-healing gel for mitigating circulation loss. *Advances in Geo-Energy Research* **8** (2023).
37. Huang, L., Xu, C., Xu, J. & Zhao, Y. Hydrate dissociation evaluation and stratum subsidence response induced by depressurization in hydrate-bearing permafrost. *Energy Fuels* **36**, 11077–11088 (2022).
38. Qin, Y., Pan, Z., Liu, Z., Shang, L. & Zhou, L. Influence of the particle size of porous media on the formation of natural gas hydrate: A review. *Energy Fuels* **35**, 11640–11664 (2021).
39. Liu, S. et al. Microstructural and hydration resistance study of CaO with powder surface modification by Al coupling agents: Alkoxy type and phosphate type. *Ceram. Int.* **47**, 18699–18707 (2021).
40. Aziz, T. et al. Recent progress in silane coupling agent with its emerging applications. *J. Polym. Environ.*, 1–17 (2021).
41. Valadez-Gonzalez, A., Cervantes-Uc, J., Olayo, R. & Herrera-Franco, P. Chemical modification of henequen fibers with an organosilane coupling agent. *Compos. Part B Eng.* **30**, 321–331 (1999).
42. Song, M. et al. Effect of viscosity and concentration of wall former, emulsifier and pore-inducer on the properties of amoxicillin microcapsules prepared by emulsion solvent evaporation. *Il Farmaco* **60**, 261–267 (2005).

43. Shibata, H. et al. Fabrication and pore size control of large-pore mesoporous silica particles through a solvent evaporation process. *Silicon* **3**, 139–143 (2011).
44. Li, G. et al. Solvent evaporation self-motivated continual synthesis of versatile porous polymer microspheres via foaming-transfer. *Colloids Surf. A Physicochem. Eng. Asp.* **615**, 126239 (2021).
45. Yu, Y. et al. An efficient preparation of porous polymeric microspheres by solvent evaporation in foam phase. *Chin. J. Chem. Eng.* **29**, 409–416 (2021).
46. Zhao, J., Milanova, M., Warmoeskerken, M. M. & Dutschk, V. Surface modification of TiO_2 nanoparticles with silane coupling agents. *Colloids Surf. A Physicochem. Eng. Asp.* **413**, 273–279 (2012).
47. Neves, R. M., Ornaghi, H. L. Jr., Zattera, A. J. & Amico, S. C. Recent studies on modified cellulose/nanocellulose epoxy composites: A systematic review. *Carbohydr. Polym.* **255**, 117366 (2021).
48. Kang, H.-J., Meesiri, W. & Blum, F. D. Nuclear magnetic resonance studies of the hydrolysis and molecular motion of aminopropylsilane. *Mater. Sci. Eng. A* **126**, 265–270 (1990).
49. Yang, Y., Wu, W., Fu, S. & Zhang, H. Study of a novel ceramsite-based shape-stabilized composite phase change material (PCM) for energy conservation in buildings. *Construct. Build. Mater.* **246**, 118479 (2020).
50. Mahmoud, M. E., Saad, E. A., Soliman, M. A. & Abdelwahab, M. S. Synthesis and surface protection of nano zerovalent iron (NZVI) with 3-aminopropyltrimethoxysilane for water remediation of cobalt and zinc and their radioactive isotopes. *RSC Adv.* **6**, 66242–66251 (2016).
51. Desai, J., Alexander, K. & Riga, A. Characterization of polymeric dispersions of dimenhydrinate in ethyl cellulose for controlled release. *Int. J. Pharm.* **308**, 115–123 (2006).
52. Wu, Z., Zhuo, Q., Sun, T. & Wang, Z. Mechanical properties of epoxy resins reinforced with synthetic boehmite (AlOOH) nanosheets. *J. Appl. Polym. Sci.* **132** (2015).
53. Li, M. et al. Permeability analysis of hydrate-bearing sediments during the hydrate formation process. *Energy Fuels* **35**, 19606–19613 (2021).
54. Wei, N. et al. Evaluation of physical parameters and construction of the classification system of natural gas hydrate in the Northern South China sea. *Energy Fuels* **35**, 7637–7645 (2021).
55. Xiao, C.-W. et al. Numerical analysis of production behaviors and permeability characteristics on the second gas hydrate production test in the South China sea. *Energy Fuels* **36**, 10960–10974 (2022).
56. Liu, W. et al. Research on evaluation and prevention of hydrate formation and blockage risk in wellbore during deepwater gas wells drilling. *J. Petrol. Sci. Eng.* **180**, 668–680 (2019).
57. Zhang, G. et al. Simulation research on solid fluidization exploitation of deepwater superficial layer natural gas hydrate reservoirs based on double-layer continuous pipe. *J. Nat. Gas Sci. Eng.* **108**, 104828 (2022).
58. Zhao, X. et al. Wellbore temperature distribution during drilling of natural gas hydrate formation in South China sea. *Petroleum* **7**, 451–459 (2021).

Acknowledgements

This work was supported by the National Key Research and Development Program of China (2021YFC2800803).

Author contributions

Jintang Wang, Jiaqi Xu, Yujing Bai and wrote the main manuscript text .Hao Xu, Guolei He, Yiyao Li, Wenbiao Li prepared Figs. 7, 8 and 9.Bo Liao prepared Fig. 1.All authors reviewed the manuscript.

Declarations

Competing interests

The authors declare no competing interests.

Additional information

Supplementary Information The online version contains supplementary material available at https://doi.org/10.1038/s41598-024-73445-1.

Correspondence and requests for materials should be addressed to H.X.